Theoretical determination of bound–free absorption cross sections in Ar_2^+ [a)]

Walter J. Stevens

Laser Physics Section 277.05, National Bureau of Standards, Boulder, Colorado 80302

Maureen Gardner and Arnold Karo

Chemistry Division, Lawrence Livermore Laboratory, Livermore, California 94505

Paul Julienne

Physical Chemistry Division, National Bureau of Standards, Washington, D.C. 20234
(Received 25 January 1977)

Ab initio calculations have been carried out for the potential energy curves and transition moments of the $^2\Sigma_u^+$, $^2\Pi_g$, $^2\Pi_u$, and $^2\Sigma_g^+$ states of Ar_2^+ which arise from the $^2P+{}^1S$ ion–atom asymptote. These data have been used in a theoretical calculation of the dissociative absorption cross sections from the bound $^2\Sigma_u^+$ state to the repulsive $^2\Pi_g$ and $^2\Sigma_g^+$ states. The $^2\Sigma_u^+ \rightarrow {}^2\Pi_g$ transition, which is dominated by spin–orbit effects, has a maximum absorption cross section of 2.6×10^{-19} cm^2 centered at 716 nm with a full width at half-maximum of 185 nm at room temperature. The $^2\Sigma_u^+ \rightarrow {}^2\Sigma_g^+$ transition is found to be much stronger with a maximum cross section of 0.5×10^{-16} cm^2 centered at 300 nm with a full width at half-maximum of 75 nm at room temperature.

I. INTRODUCTION

Because of their ready availability, inertness, and high stopping power rare-gas species are commonly used in electron-beam and high-energy discharge experiments as converters of electron energy to atomic and molecular excitation energy. High pressure rare-gas systems excited in this way have been used as efficient fluorescers and as uv gas lasers.[1] More recently, there has been a growing interest in the use of rare gases as energy reservoirs with subsequent collisional transfer of the stored energy to the principal lasing component of a mixed gas laser system. This technique has been used to produce lasers based on the oxygen atom ^1S–^1D transition in rare-gas/O_2 mixtures,[2] and also is the basis of the newly developed rare-gas/halide laser systems.

Recently, several reports have indicated the existence of strong optical absorption cross sections throughout the visible and uv in high pressure rare gases excited by electron beams.[3] These absorptions act as gain inhibitors in electron-beam pumped rare-gas/oxygen laser systems. At high enough pressures after initial ionization of the rare-gas atoms by the electron beam transient ground state molecular ions such as Ar_2^+, Kr_2^+, and Xe_2^+ are formed, and it has been suggested that photodissociation of these species may be responsible for at least part of the observed visible and uv absorption cross sections. The photodissociation occurs by optical transitions from the bound states of these ions to higher lying repulsive states, and would therefore appear as broad-band, continuum absorptions. These bound–free transitions are expected in many instances to fall within the visible range of the spectrum.

The difficulties associated with the experimental determination of absolute absorption cross sections have been discussed recently by Miller *et al.*[4] in a series of measurements of the absolute total photodissociation cross sections for a number of molecular ions including Ar_2^+, Kr_2^+, and Xe_2^+. They report that, in addition to a 6% statistical uncertainty in the ion intensity measurements, a 25% uncertainty should be ascribed to their procedure for normalizing to the absolute photodetachment cross section of O_2^-. Theoretical calculations were also reported in the same paper for the relative magnitude of the photodissociation cross section for the $^2\Sigma_u^+ \rightarrow {}^2\Pi_g$ transition in the Ar_2^+ as a function of wavelength. In those calculations the assumption was made that the transition dipole moment is independent of internuclear separation over the small range of interatomic distance associated with the $^2\Sigma_u^+ \rightarrow {}^2\Pi_g$ transition. Also, no measurements or calculations were made for the $^2\Sigma_u^+ \rightarrow {}^2\Sigma_g^+$ dissociative transition.

The present work has retained the single-configuration (restricted Hartree–Fock) representation of the molecular wavefunction as in the earlier calculations of Gilbert and Wahl.[5] However, a more extensive basis set has been used when compared to that work,[5] from which the Ar_2^+ potential curves used by Miller *et al.*[4] were taken. In addition, the dependence of the transition moment on internuclear distance has been included in the determination of the absorption cross sections for both the $^2\Sigma_u^+ \rightarrow {}^2\Pi_g$ transition and the much more intense $^2\Sigma_u^+ \rightarrow {}^2\Sigma_g^+$ transition occurring at shorter wavelengths.

II. CALCULATION OF THE POTENTIAL ENERGY CURVES

A. Method

In the present work the wavefunctions and energies associated with the $^2\Sigma_u^+$, $^2\Pi_g$, $^2\Pi_u$, and $^2\Sigma_g^+$ states of Ar_2^+ have been determined over a wide range of interatomic separations using standard procedures and computer programs which have been fully described elsewhere.[6] The basis set of Slater-type functions (STF) used in the calculations is listed in Table I and was developed from

[a)]Research supported by the U.S. Energy Research and Development Administration under contract number E(49-1)-3800.

TABLE I. Slater-type function basis set for Ar_2^+.[a]

Block	Type	N	L	M	Zeta
Sigma	$1s$	1	0	0	19.250
	$2s$	2	0	0	16.781
	$3s$	3	0	0	11.191
	$2s$	2	0	0	6.332
	$3s$	3	0	0	3.143
	$3s$	3	0	0	1.980
	$4s$	4	0	0	1.199
	$4s$	4	0	0	0.695
	$2p$	2	1	0	15.317
	$2p$	2	1	0	9.053
	$2p$	2	1	0	5.770
	$3p$	3	1	0	2.893
	$3p$	3	1	0	1.605
	$4p$	4	1	0	0.800
	$3d$	3	2	0	2.000
Pi	$2p$	2	1	1	15.317
	$2p$	2	1	1	9.053
	$2p$	2	1	1	5.770
	$3p$	3	1	1	2.893
	$3p$	3	1	1	1.605
	$4p$	4	1	1	0.800
	$3d$	3	2	1	2.000

[a]Slater-type functions are defined by

$$X_{NLM} = A_N r^{N-1} e^{-\zeta r} Y_{LM}(\theta, \phi) ,$$

where A_N is a normalization factor and Y_{LM} is the usual spherical harmonic. Identical sets of functions were placed at each nuclear center.

a nominal atomic basis[7] augmented with $3d$, $4s$, and $4p$ functions chosen to provide a more accurate description of the atomic polarization effects. It is now well recognized that carefully optimized atomic basis sets of reasonable size form reliable starting points for molecular calculations. In addition, previous experience has shown that a well-constructed basis set for the neutral atom should give reliable results for the positive ion in the molecular region as well.

The following single configurations were used to describe the four Ar_2^+ electronic states arising from the Ar (^1S) and Ar^+ (^2P) atomic states:

$$\begin{aligned} {}^2\Sigma_u^+ &= [\text{core}]\,(3p\sigma_g)^2\,(3p\sigma_u)^1\,(3p\pi_u)^4\,(3p\pi_g)^4 , \\ {}^2\Sigma_g^+ &= [\text{core}]\,(3p\sigma_g)^1\,(3p\sigma_u)^2\,(3p\pi_u)^4\,(3p\pi_g)^4 , \\ {}^2\Pi_g &= [\text{core}]\,(3p\sigma_g)^2\,(3p\sigma_u)^2\,(3p\pi_u)^4\,(3p\pi_g)^3 , \\ {}^2\Pi_u &= [\text{core}]\,(3p\sigma_g)^2\,(3p\sigma_u)^2\,(3p\pi_u)^3\,(3p\pi_g)^4 . \end{aligned} \qquad \text{(II. 1)}$$

The single-configuration wavefunctions are sufficient to provide a formally correct description of the dissociation of the molecular ion into the appropriate atomic fragments. However, because of the homonuclear character of the dimer, the restricted Hartree–Fock description requires the dissociated atom and atomic ion to have exactly the same core electronic distribution. This restriction causes the computed asymptotic energy to be seriously in error. This effect has been discussed in detail by Gilbert and Wahl in their earlier work.[5] There appears to be some cancellation between the asymptotic errors and the molecular correlation energies which are not accounted for by the single configuration wavefunction. The good agreement between the calculated and experimental[8] values for D_e and R_e of the $^2\Sigma_u^+$ state lends credibility to this argument. However, the core restrictions remain the primary source of error in our calculations.

The $^2\Sigma_u^+$ state is expected to be lowest in energy and should exhibit an attractive potential. Based on the estimates of Mulliken[9] the $^2\Pi_g$, $^2\Pi_u$, and $^2\Sigma_g^+$ states should be found to have repulsive potentials and lie above the $^2\Sigma_u^+$ ground state in the order listed. Gilbert and Wahl have published a single-configuration *ab initio* calculation for the $^2\Sigma_u^+$ state,[5] and their unpublished results for the three repulsive states have been reported in the compendium of Krauss.[10] A somewhat smaller basis set than the present one was used in the earlier work. We have used a larger basis set in anticipation that the transition moments would be more sensitive to deficiencies in the basis, and we wished, as well, to describe as accurately as possible the long-range charge–induced dipole interactions which could lead to flattening of the repulsive potentials and could significantly affect both the depth and position of any excited potential minima.

B. Results

The total energy values computed over a range of internuclear distances from 3.0 to 20.0 bohr (1 bohr $= 0.5291772 \times 10^{-8}$ cm) are summarized in Table II for the four electronic states of Ar_2^+ that were considered. The two Σ and two Π states are seen to have essentially reached the asymptotic energy when the interatomic separation is greater than 20 bohr. The difference in the two asymptotes of 0.00056 hartree (1 hartree = 219 475 cm^{-1}) results from the well-known inequivalence of the $p\sigma$ and $p\pi$ orbitals in open-shell systems in $C_{\infty v}$ symmetry. In Fig. 1 we have plotted the potential energy curves derived from the total molecular energies along with the results of Gilbert and Wahl.[5] In the plot, and in the absorption cross-section calculations to follow, the asymptotic energies of the four states (at 20 bohr) were set equal to zero.

TABLE II. Total energy values (in hartree)[a] for the $X\,^2\Sigma_u^+$, $^2\Pi_g$, $^2\Pi_u$, and $^2\Sigma_g^+$ states of Ar_2^+ as a function of internuclear distance R (in bohr).[b]

R	$^2\Sigma_u^+$	$^2\Pi_g$	$^2\Pi_u$	$^2\Sigma_g^+$
3.0	−1052.73306			
4.0	−1053.08515	−1052.96997	−1052.89600	−1052.81741
4.25	−1053.10138	−1053.00907	−1052.95360	−1052.88442
4.5	−1053.10761	−1053.03333	−1052.99171	−1052.93244
4.75	−1053.10799	−1053.04802	−1053.01677	−1052.96697
5.0	−1053.10519	−1053.05667	−1053.03319	−1052.99196
5.5	−1053.09602	−1053.06417	−1053.05090	−1053.02356
6.5	−1053.07953	−1053.06585	−1053.06162	−1053.05071
7.0	−1053.07431	−1053.06536	−1053.06298	−1053.05642
12.0	−1053.06445	−1053.06378	−1053.06377	−1053.06434
20.0	−1053.06421	−1053.06364	−1053.06364	−1053.06420

[a]1 hartree = 27.212 eV = 219 475 cm^{-1}.
[b]1 bohr = 0.5291772×10^{-8} cm.

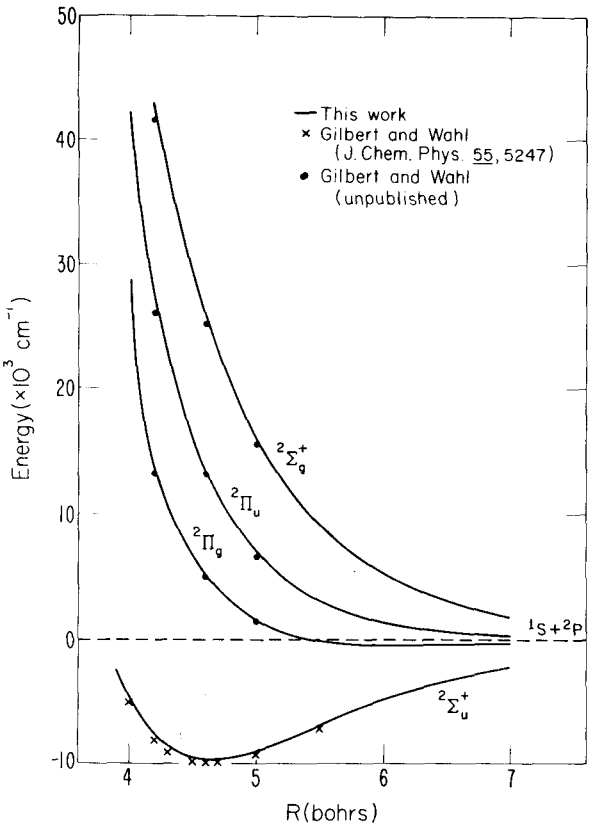

FIG. 1. *Ab initio* potential energy curves for the states of Ar_2^+ arising from the $Ar^+(^2P) + Ar(^1S)$ asymptote (1 bohr = 0.5291772 $\times 10^{-8}$ cm).

These results show that the $X\,^2\Sigma_u^+$ state exhibits an attractive potential, bound by about 1.2 eV at the equilibrium interatomic separation of 4.65 bohr. This is consistent with earlier calculations of Gilbert and Wahl,[5] who obtained values of $D_e = 1.25$ eV and $R_e = 4.6$ bohr. These values are also in agreement with the low-energy elastic differential cross-section results of Lorents *et al.*,[8] whose rainbow scattering data were consistent with a well depth of 1.25 eV and an equilibrium separation of 4.6 bohr, and with the potential curve derived from the ion–atom scattering data of Mittmann and Weise,[11] who found values of $D_e = 1.34$ eV and $R_e = 4.6$ bohr. The experimental data are not sensitive in first order to the value of R_e.

The three other electronic states investigated lie above the $^2\Sigma_u^+$ ground state in the order $^2\Pi_g$, $^2\Pi_u$, and $^2\Sigma_g^+$. The $^2\Pi_g$ state has a shallow minimum equal to ≈ 0.06 eV at 6.4 bohr. This is entirely reasonable when compared with the value of 0.25 eV estimated for the corresponding $^2\Pi_g$ state of Xe_2^+.[12]

Dissociative dipole transitions from the $^2\Sigma_u^+$ ground state are allowed to the repulsive $^2\Pi_g$ and $^2\Sigma_g^+$ states. The arrangement of the potential curves in Fig. 1 shows that these transitions should be broad-band continua, widely separated in wavelength.

C. Spin–orbit effects

The *ab initio* calculations described above do not include the effects of spin–orbit coupling. The spin–orbit effects can be accounted for in an approximate way by assuming that the molecular wavefunctions are represented approximately by products of atomic wavefunctions (PAW) at all internuclear separations. The appropriate atomic states can be represented by $|L, S, \Lambda, \Sigma\rangle$, where Λ and Σ are the respective projections of angular momentum and spin on the molecular axis. The molecular states are then written as

$$\psi_{g,u}(\Lambda, \Sigma) = \frac{1}{\sqrt{2}} \left(|0, 0, 0, 0\rangle_A |L, S, \Lambda, \Sigma\rangle_B \pm |L, S, \Lambda, \Sigma\rangle_A |0, 0, 0, 0\rangle_B \right), \quad \text{(II. 2)}$$

where $|0, 0, 0, 0\rangle$ is the ground state argon atom, A and B refer to the two nuclear centers, and the + and − linear combinations refer to the gerade and ungerade Ar_2^+ states, respectively.

The toal molecular electronic Hamiltonian is

$$H = H_{AB} + H_{SO}, \quad \text{(II. 3)}$$

where H_{AB} is the spinfree Hamiltonian used in the calculations described in the sections above, and H_{SO} is the molecular spin–orbit operator which in the PAW approximation is simply a sum of the spin–orbit operators for each atom

$$H_{SO} = H_{SO}^A + H_{SO}^B. \quad \text{(II. 4)}$$

The matrix elements of the atomic spin–orbit operators are given by

$$V_{SO} = \sum_i \alpha_i \mathbf{l}_i \cdot \mathbf{s}_i. \quad \text{(II. 5)}$$

For Ar^+, with five equivalent p electrons, we can write

$$V_{SO} = \alpha \mathbf{L} \cdot \mathbf{S}. \quad \text{(II. 6)}$$

The spin–orbit coupling constant α may be obtained by fitting the observed splitting of the $^2P_{3/2}$ and $^2P_{1/2}$ states of Ar^+. A good fit is obtained for $\alpha = -955$ cm^{-1}. The atomic spin–orbit operator is diagonal for atomic states in the total angular momentum representation $|L, S, J, \Omega\rangle$, where $\mathbf{J} = \mathbf{L} + \mathbf{S}$ and Ω is the projection of $\mathbf{J}$. The $|L, S, \Lambda, \Sigma\rangle$ states can be expanded in this representation

$$|L, S, \Lambda, \Sigma\rangle = \sum_J (L, S, J | \Lambda, \Sigma, \Omega) |L, S, J, \Omega\rangle, \quad \text{(II. 7)}$$

where $(L, S, J | \Lambda, \Sigma, \Omega)$ are the Clebsch–Gordan coefficients and $\Omega = \Lambda + \Sigma$.

At this point it is easy to set up the total molecular electronic Hamiltonian matrix in the PAW approximation. Using the molecular wavefunctions as given by Eq. (II. 2) we have

$$\begin{matrix} |\Omega| = \frac{1}{2} \\ |\Omega| = \frac{1}{2} \\ |\Omega| = \frac{3}{2} \end{matrix} \begin{bmatrix} E(^2\Pi) - \frac{1}{2}\alpha & \sqrt{\frac{1}{2}}\alpha & 0 \\ \sqrt{\frac{1}{2}}\alpha & E(^2\Sigma) & 0 \\ 0 & 0 & E(^2\Pi) + \alpha \end{bmatrix}, \quad \text{(II. 8)}$$

where $E(^2\Pi)$ and $E(^2\Sigma)$ are the eigenfunctions of H_{AB} which have already been calculated for several internuclear separations, and α is the atomic spin–orbit matrix element which is assumed to be independent of internuclear separation. This matrix obtains for both the gerade and ungerade states. The eigenfunctions of Eq.

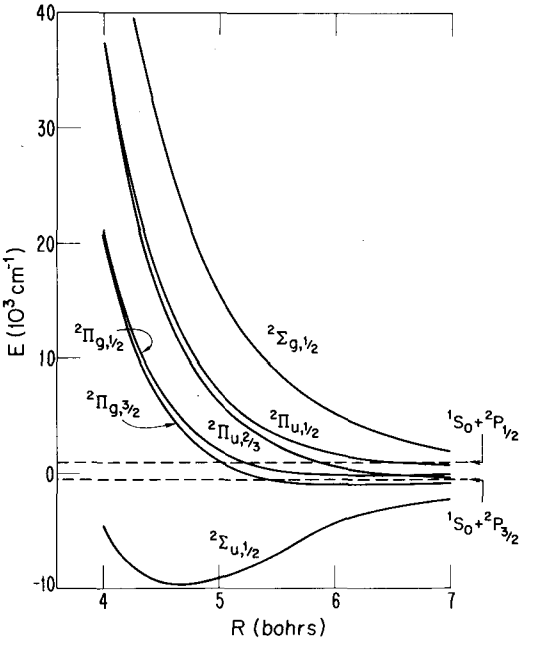

FIG. 2. Ar_2^+ potential energy curves including spin–orbit coupling effects (1 bohr = 0.5291772×10^{-8} cm).

(II. 8) are the molecular electronic energies including spin–orbit coupling, and the eigenvalues give the mixing of the $^2\Sigma$ and $^2\Pi$ states. In general, we will have for the gerade (g) states

$$|^2\Sigma_{g,1/2}\rangle = a_g|^2\Sigma_g\rangle + b_g|^2\Pi_g\rangle\ , \qquad \text{(II. 9a)}$$

$$|^2\Pi_{g,3/2}\rangle = |^2\Pi_g\rangle\ , \qquad \text{(II. 9b)}$$

$$|^2\Pi_{g,1/2}\rangle = a_g'|^2\Pi_g\rangle + b_g'|^2\Sigma_g\rangle\ , \qquad \text{(II. 9c)}$$

where the subscripts $\frac{1}{2}$ and $\frac{3}{2}$ refer to the value of $\Omega = \Lambda + \Sigma$. The coefficients a_g and a_g' should be near unity, while b_g and b_g' should be very small. Identical equations hold for the ungerade states. From here on we will let the unprimed coefficients represent the sigma states and the primed coefficients represent the pi states.

The potential energy curves resulting from the diagonalization of Eq. (II. 8) are shown in Fig. 2. The spin–orbit splitting near R_e is seen to be small compared to the $\Sigma-\Pi$ splitting. The mixing of the Σ and Π states is shown in Table III. Although the mixing is very small, it has a significant effect on the computed absorption cross sections for the $\Sigma \rightarrow \Pi$ transition as discussed below in Sec. IV.

TABLE IV. Transition moments (in a.u.)[a] for the states of Ar_2^+ arising from the $^1S+^2P$ atom–ion asymptote.

R(bohr)[b]	$^2\Sigma_u^+ \rightarrow {}^2\Pi_g$[c]	$^2\Sigma_u^+ \rightarrow {}^2\Sigma_g^+$	$^2\Pi_u \rightarrow {}^2\Pi_g$	$^2\Pi_u \rightarrow {}^2\Sigma_g^+$[c]
4.00	0.066	1.974	1.955	−0.064
4.25	0.053	2.085	2.088	−0.037
4.50	0.042	2.198	2.220	−0.017
4.75	0.034	2.313	2.350	−0.004
5.00	0.028	2.432	2.478	0.005
5.50	0.020	2.676	2.733	0.014
6.50	0.012	3.184	3.237	0.016
7.00	0.011	3.441	3.489	0.014
12.00	0.004	5.978	5.995	0.004
20.00	0.002	9.988	9.996	0.002

[a]1 a.u. = 6.4606 (D)^2.
[b]1 bohr = 0.5291772×10^{-8} cm.
[c]This transition moment does not include the factor of 2 degeneracy for the pi state electronic angular momentum.

III. TRANSITION MOMENTS

With the potential energy curves for each state well characterized as a function of internuclear distance the dipole transition moments were then evaluated as a function of internuclear distance for the $^2\Sigma_u^+ - {}^2\Pi_g$ and $^2\Sigma_u^+ - {}^2\Sigma_g^+$ transitions, which are of primary concern, and for the $^2\Pi_u - {}^2\Pi_g$ and $^2\Pi_u - {}^2\Sigma_g^+$ transitions as well. The moments were evaluated in the dipole length form, and are tabulated in Table IV.

The $^2\Sigma_u^+ - {}^2\Pi_g$ and $^2\Sigma_u^+ - {}^2\Sigma_g^+$ transition moments are plotted in Fig. 3. They show a strong dependence on R over the entire range for the $^2\Sigma_u^+ - {}^2\Sigma_g^+$ transition and in the region $3.0 \le R \le 8.0$ bohr for the $^2\Sigma_u^+ - {}^2\Pi_g$ transition. The $^2\Sigma_u^+ - {}^2\Sigma_g^+$ transition can be seen to be the much stronger of the two. It is also interesting to observe that while the transition matrix elements go to zero at large R for the $^2\Sigma_u^+ - {}^2\Pi_g$ transition, the $^2\Sigma_u^+ - {}^2\Sigma_g^+$ values scale as R. At large R the moment for this transition becomes equal to $R/2$. The reason for this behavior can be seen as follows: Asymptotically, the transition moment for $Ar_2 + {}^2\Sigma_u^+ - {}^2\Sigma_g^+$ can be written

$$\mu = \langle \Psi_g|\,\mathbf{z}\,|\Psi_u\rangle = \tfrac{1}{2}\langle (p_a + p_b)|\,\mathbf{z}\,|(p_a - p_b)\rangle$$
$$= \tfrac{1}{2}[\langle p_a|\,\mathbf{z}\,|p_a\rangle - \langle p_b|\,\mathbf{z}\,|p_b\rangle]\ , \qquad \text{(III. 1)}$$

TABLE III. Ar_2^+ spin–orbit mixing coefficients.

	$^2\Sigma_{u,1/2}^+$		$^2\Pi_{u,1/2}$		$^2\Pi_{g,1/2}$		$^2\Sigma_{g,1/2}^+$	
R(bohr)[a]	Σ	Π	Σ	Π	Σ	Π	Σ	Π
4.00	0.99987	0.01611	−0.01611	0.99987	0.02035	0.99979	0.99979	−0.02035
4.25	0.99979	0.02056	−0.02056	0.99979	0.02496	0.99969	0.99969	−0.02496
4.50	0.99966	0.02613	−0.02613	0.99966	0.03092	0.99952	0.99952	−0.03092
4.75	0.99945	0.03306	−0.03306	0.99945	0.03861	0.99925	0.99925	−0.03861
5.00	0.99913	0.04165	−0.04165	0.99913	0.04880	0.99881	0.99881	−0.04880
5.50	0.99786	0.06536	−0.06536	0.99786	0.07809	0.99695	0.99695	−0.07809
6.50	0.98838	0.15200	−0.15200	0.98838	0.21166	0.97734	0.97734	−0.21166
7.00	0.97549	0.22003	−0.22003	0.97549	0.33514	0.94217	0.94217	−0.33514

[a]1 bohr = 0.5291772 Å.

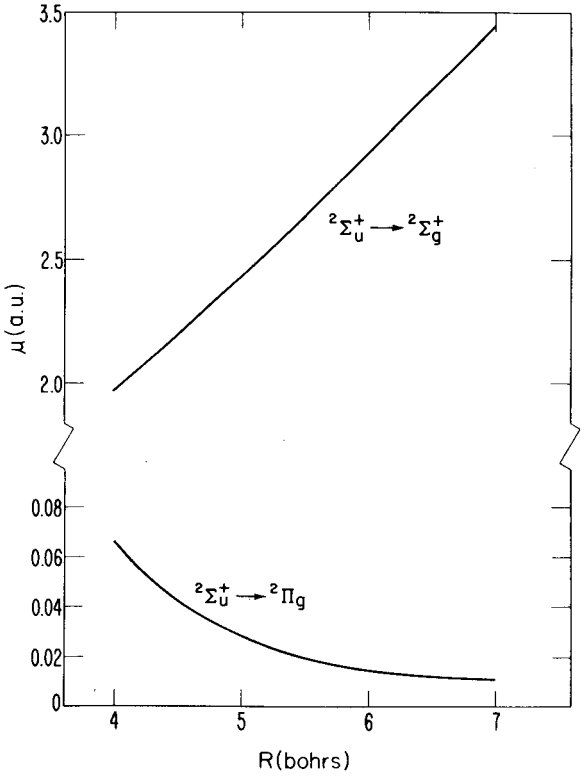

FIG. 3. Calculated transition dipole moments for transitions from the $^2\Sigma_u^+$ ground state of Ar_2^+ (1 a.u. = 2.5418×10^{-18} esu cm; 1 bohr = 0.5291772×10^{-8} cm).

where we have used the wavefunction definitions of Eq. (II.1). The matrix elements $\langle p_a|z|p_b\rangle$ and $\langle p_b|z|p_a\rangle$, which vanish at large R, also cancel at intermediate interatomic distances where there is overlap. Thus, the transition moment at large R, for this case, becomes a direct measure of the charge separation, or $|\mu| \sim \frac{1}{2}R$. Small deviations do occur because the p orbitals are distorted slightly by charge-induced dipole effects. The exact transition moment at large R would deviate significantly from this simple $R/2$ relationship because of configuration interaction and spin-orbit mixing.

Our results for the $^2\Sigma_u^+ - {}^2\Pi_g$ transition moment can be compared to the calculations of Miller *et al.*[4] Although they didn't explicitly evaluate the transition moment from molecular wavefunctions, they estimated that a value of $|\mu|^2 = 0.0045$ a.u.[13] (1 a.u. = 6.45 D^2) is necessary to achieve agreement between theoretically and experimentally determined cross sections for the $^2\Sigma_u^+ - {}^2\Pi_g$ transition. Our computed value for $|\mu|^2$ near R_e of the $^2\Sigma_u^+$ state is 0.00137 a.u. Our value does not include spin-orbit effects, which are substantial for this transition as indicated below. The transition moment of Miller *et al.*[4] implicitly includes spin-orbit effects since it was derived from experimental data.

IV. ABSORPTION CROSS SECTIONS

A. Method

Given the potential energy curves and transition moments for the states in question computing the absorption cross sections is a straightforward task if the vibrational and continuum wavefunctions can be generated. The theory outlined below shall be formulated to include the effects of spin-orbit mixing between the $^2\Sigma$ and $^2\Pi$ states. For an isolated diatomic molecule the total parity P and the total angular momentum J (electronic + spin + nuclear rotation) and its space-fixed projection M are exact quantum numbers. Let us assume also that the molecule-fixed projection Ω of electronic angular momentum (space and spin components) is an approximately good quantum number. States of the same Ω are mixed by spin-orbit coupling, whereas states differing in Ω by ±1 are only mixed by electronic-rotation and spin-rotation coupling terms. These latter terms are both approximately proportional to B_eJ, where B_e is the equilibrium rotational constant of the molecule. Since $B_eJ \lesssim 10$ cm^{-1} for thermal J's in Ar_2^+ and since the spin-orbit matrix elements in Ar_2^+ are of the order of 10^3 cm^{-1}, it is safe to neglect rotational uncoupling effects in comparison to spin-orbit mixing in calculating photodissociation cross sections for sufficiently low temperatures, say $T \lesssim 1000$ K. Thus, the spin-orbit effects can be approximated as in Sec. II C.

The photodissociation cross section at wavelength λ for absorption from the initial level i characterized by quantum numbers $JMv\Omega P$ to the final continuum state f characterized by $J'M'\epsilon\Omega'P'$ is (here Ω means $|\Omega|$; the $|\Omega P\rangle$ wavefunctions with parity are comprised of $\pm|\Omega|$ components)

$$\sigma_\lambda(i\rightarrow f) = \frac{8\pi^3}{3\lambda}\,\left|\langle JMv\Omega P|\,\mu_{sp}|\,J'M'\epsilon\Omega'P'\rangle\right|^2, \qquad \text{(IV.1)}$$

where μ_{sp} is the dipole operator in a space-fixed coordinate frame in esu cm. The continuum channel is described here in the conventional manner in terms of a single electronic state with electronic angular momentum projection Ω'. The radial "vibrational" continuum functions are assumed to be energy normalized

$$\langle\epsilon_1|\,\epsilon_2\rangle = \delta(\epsilon_1 - \epsilon_2)\,. \qquad \text{(IV.2)}$$

In general, the continuum functions must be constructed as solutions to a multichannel scattering problem with the appropriate boundary conditions. This is a nontrivial problem for the case of electronically degenerate fragment atoms. The single channel approximation is believed to be adequate for the problem at hand, where the fragment kinetic energy at the photodissociation peak is significantly larger than the asymptotic fine structure splitting.

A meaningful comparison with experiment requires the average cross section for absorption from an ensemble of initial states. Here we will utilize a thermal ensemble of populations, namely,

$$\frac{N_{JMv\Omega P}}{N} = \frac{1}{Q_T}\exp(-E_{vJP}/kT)\,, \qquad \text{(IV.3)}$$

where Q_T is the $^2\Sigma_u^+$ vibration-rotation partition function (including electronic spin degeneracy) at temperature T, N is the total number of ground state molecules, and E_{vJP} is the energy of the ground state vibrational rotational level. The total average cross section including a sum over all final states is

$$\sigma_\lambda = \frac{1}{N}\sum_{if} N_i \sigma_\lambda(i \to f)$$
$$= \frac{8\pi^3}{3\lambda}\sum_{vJP}\frac{1}{Q_T}\exp(-E_{vJP}/kT)$$
$$\times \sum_{\substack{MM'\\ J'\Omega' P'}} |\langle JMv\Omega P|\, \mu_{sp}\, |J'M'\epsilon_\lambda\Omega' P'\rangle|^2 . \quad \text{(IV. 4)}$$

The final state energy ϵ_λ is related to λ and the initial state energy E_{vJP} by energy conservation

$$\epsilon_\lambda = E_{vJP} + (hc/\lambda) . \quad \text{(IV. 5)}$$

Only final states with $P' = -P$ contribute to the dipole matrix elements in Eq. (IV. 4). The summation over M and M' can be carried out in a straightforward manner by expanding μ_{sp} in the components of the dipole operator in the molecule-fixed coordinate frame and utilizing the well-known properties of the rotation matrices and the Clebsch–Gordan coefficients. The result is

$$\sigma_\lambda = \frac{8\pi^3}{3\lambda}\sum_{vJP}(2J+1)\frac{1}{Q_T}\exp(-E_{vJP}/kT)$$
$$\times \sum_{J'\Omega'} S(Jv\Omega \to J'\epsilon_\lambda\Omega') , \quad \text{(IV. 6)}$$

where for the $\Omega = \frac{1}{2} \to \Omega' = \frac{1}{2}$ transitions

$$S(Jv\tfrac{1}{2} \to J'\epsilon_\lambda\tfrac{1}{2}) = |(J1J'|\tfrac{1}{2}0\tfrac{1}{2})\langle vJ|\, T_0\,|\epsilon_\lambda J'\rangle$$
$$- (J1J'|-\tfrac{1}{2}1\tfrac{1}{2})\langle vJ|\, T_1\,|\epsilon_\lambda J'\rangle|^2 \quad \text{(IV. 7)}$$

and for $\Omega = \frac{1}{2} \to \Omega' = \frac{3}{2}$ transitions

$$S(Jv\tfrac{1}{2} \to J'\epsilon_\lambda\tfrac{3}{2}) = (J1J'|\tfrac{1}{2}1\tfrac{3}{2})^2|\langle vJ|\, T_1'\,|\epsilon_\lambda J'\rangle|^2 , \quad \text{(IV. 8)}$$

where the terms $(J1J'|\Omega 1\Omega')$ and $(J1J'|\Omega 0\Omega')$ are the Clebsch–Gordan coefficients. The matrix elements of the molecule-fixed electronic dipole operator for the $^2\Sigma_u \to {}^2\Pi_g$ transition in terms of the spin–orbit mixed electronic states are

$$T_0 = \langle {}^2\Sigma^+_{u,\pm 1/2}|\, \mu_0\, |{}^2\Pi_{g,\pm 1/2}\rangle , \quad \text{(IV. 9a)}$$
$$T_1 = \langle {}^2\Sigma^+_{u,\pm 1/2}|\, \mu_{\pm 1}\, |{}^2\Pi_{g,\mp 1/2}\rangle , \quad \text{(IV. 9b)}$$
$$T_1' = \langle {}^2\Sigma^+_{u,\pm 1/2}|\, \mu_{\mp 1}\, |{}^2\Pi_{g,\pm 3/2}\rangle , \quad \text{(IV. 9c)}$$

where

$$\mu_{\pm 1} = (\mp \mu_x - i\mu_y)/\sqrt{2} \quad \text{(IV. 10)}$$

is the dipole operator in the molecule-fixed coordinate frame. For the $^2\Sigma_u \to {}^2\Sigma_g$ transition there is no $|\Omega|' = \frac{3}{2}$ component and we only have Eq. (IV. 7) for which the dipole matrix elements are

$$T_0 = \langle {}^2\Sigma^+_{u,\pm 1/2}|\, \mu_0\, |{}^2\Sigma^+_{g,\pm 1/2}\rangle , \quad \text{(IV. 11a)}$$
$$T_1 = \langle {}^2\Sigma^+_{u,\pm 1/2}|\, \mu_{\pm 1}\, |{}^2\Sigma^+_{g,\mp 1/2}\rangle . \quad \text{(IV. 11b)}$$

A $\frac{1}{2} \to \frac{1}{2}$ transition is unique among $|\Omega| = |\Omega'|$ transitions in that both parallel (T_0) and perpendicular (T_1) transitions can contribute to the transition amplitude as in Eq. (IV. 7) when $\Omega = \frac{1}{2}$ states with $\Lambda = 0$ and 1 are mixed by the spin–orbit interaction. This has a pronounced effect on the computed $^2\Sigma_u^+ \to {}^2\Pi_g$ absorption cross sections and is discussed in more detail in a section below.

Since Ω' is assumed to be a good quantum number, the T_1 and T_1' components of the $^2\Sigma_u^+ \to {}^2\Pi_g$ transition are independent. An interference between the T_1 and T_1' components would occur at very large J' due to the neglected spin–rotation ($\mathbf{J}\cdot\mathbf{S}$) terms which would mix $^2\Pi_{g,1/2}$ and $^2\Pi_{g,3/2}$. This effect is not being considered in the current approximation due to the smallness of the spin–rotation matrix element.

The matrix elements T can be expressed in terms of the calculated transition moments of Sec. III by using the wavefunction representations of Eqs. (II. 9). For the $^2\Sigma_u^+ \to {}^2\Pi_g$ transition we have

$$T_0 = a_u b_g' \langle {}^2\Sigma_u^+|\, \mu_0\, |{}^2\Sigma_g^+\rangle + a_g' b_u \langle {}^2\Pi_u|\, \mu_0\, |{}^2\Pi_g\rangle , \quad \text{(IV. 12a)}$$
$$T_1 = a_u a_g' \langle {}^2\Sigma_u^+|\, \mu_1\, |{}^2\Pi_g\rangle + b_u b_g' \langle {}^2\Pi_u|\, \mu_1\, |{}^2\Sigma_g^+\rangle , \quad \text{(IV. 12b)}$$
$$T_1' = a_u \langle {}^2\Sigma_u^+|\, \mu_1\, |{}^2\Pi_g\rangle . \quad \text{(IV. 12c)}$$

For the $^2\Sigma_u^+ \to {}^2\Sigma_g^+$ transition

$$T_0 = a_u a_g \langle {}^2\Sigma_u^+|\, \mu_0\, |{}^2\Sigma_g^+\rangle + b_u b_g \langle {}^2\Pi_u|\, \mu_0\, |{}^2\Pi_g\rangle , \quad \text{(IV. 13a)}$$
$$T_1 = a_u b_g \langle {}^2\Sigma_u^+|\, \mu_1\, |{}^2\Pi_g\rangle + b_u a_g \langle {}^2\Pi_u|\, \mu_{-1}\, |{}^2\Sigma_g^+\rangle . \quad \text{(IV. 13b)}$$

The expressions (IV. 7) and (IV. 8) can be greatly simplified by two additional approximations. First, assume the matrix elements $\langle vJ|\, T\,|\epsilon J'\rangle$ are independent of whether $J' = J$ or $J \pm 1$. This is a quite good approximation for Ar_2^+. Then the summation over J' can be carried out using the orthogonality properties of the Clebsch–Gordan coefficients. (To put it another way, we sum over Hönl–London factors.) In particular, the interference between the T_0 and T_1 terms in Eq. (IV. 7) is eliminated by summing over J'. The result is

$$S(Jv\tfrac{1}{2} \to J\epsilon_\lambda\tfrac{1}{2}) = |\langle vJ|\, T_0\,|\epsilon_\lambda J\rangle|^2 + |\langle vJ|\, T_1\,|\epsilon_\lambda J\rangle|^2 , \quad \text{(IV. 14a)}$$
$$S(Jv\tfrac{1}{2} \to J\epsilon_\lambda\tfrac{3}{2}) = |\langle vJ|\, T_1'\,|\epsilon_\lambda J\rangle|^2 . \quad \text{(IV. 14b)}$$

The second approximation is to neglect the centrifugal distortion of the $\langle vJ|\, T\,|\epsilon J\rangle$ matrix elements, i. e.,

$$\langle vJ|\, T\,|\epsilon J\rangle = \langle v|\, T\,|\epsilon\rangle . \quad \text{(IV. 15)}$$

This approximation is checked numerically in a section below.

These approximations lead to the expression

$$\sigma_\lambda = \frac{8\pi^3}{3\lambda}\sum_{vJP}(2J+1)\frac{1}{Q_T}$$
$$\times \exp(-E_{vJP}/kT)\sum_{\Omega'} S(v\Omega \to \epsilon_\lambda\Omega') , \quad \text{(IV. 16)}$$

where S is given by Eqs. (IV. 14) and (IV. 15). Since it is a good approximation to write $Q_T = 2Q_{vib}Q_{rot}$, where the factor 2 is due to the nearly degenerate opposite parity sublevels of the $^2\Sigma_u^+$ state, we see immediately that

$$\sigma_\lambda = \frac{8\pi^3}{3\lambda}\frac{1}{Q_{vib}}\sum_{v,\Omega'}\exp(-E_v/kT)S(v\Omega \to \epsilon_\lambda\Omega') . \quad \text{(IV. 17)}$$

The final expression for σ_λ is obtained by expressing Q_{vib} by the harmonic oscillator partition function

$$Q_{vib} = \frac{1}{1 - e^{-\omega_e/kT}} \quad \text{(IV. 16)}$$

if the temperature is not too high. In the numerical calculation of σ the matrix elements $\langle v|\, T\,|\epsilon\rangle$ were calculated using bound vibrational wavefunctions and energy-normalized single-channel continuum wavefunctions gen-

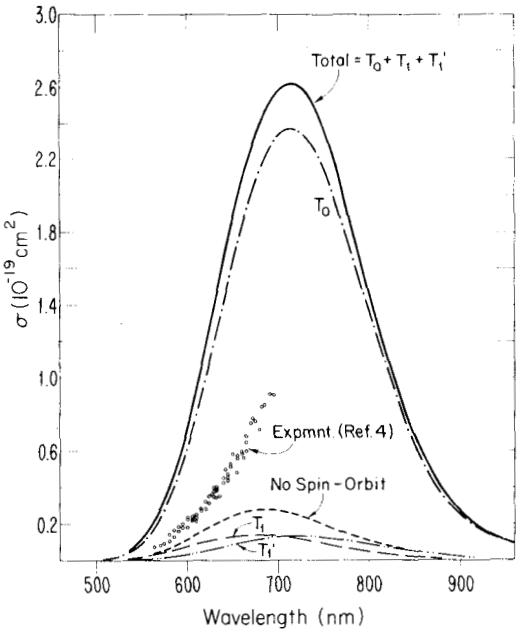

FIG. 4. Absorption cross sections for the $^2\Sigma_u^+ \rightarrow {}^2\Pi_g$ transition in Ar_2^+ at 300 K. The dots represent the laser-induced photodissociation measurements of Miller *et al.* (Ref. 4).

erated by the method of Gordon[14] using the potentials shown in Fig. 2. The vibration constant ω_e for the $^2\Sigma_u^+$ state is 300 cm^{-1} in all the calculations described below. The effect of spin–orbit coupling was investigated by setting the coefficients a and a' equal to one and the coefficients b and b' equal to zero.

B. Results

1. The $^2\Sigma_u^+ \rightarrow {}^2\Pi_g$ transition

Figure 4 shows the results of our absorption cross-section calculations for the $^2\Sigma_u^+ \rightarrow {}^2\Pi_g$ transition at 300 K, and also the experimental data of Miller *et al.* taken from Ref. 4. The cross-section calculation without spin–orbit coupling is seen to be much too small. The three components of Eq. (IV.14a) which result from the spin–orbit calculation are also shown in the figure. The T_1 and T_1' components, which include the $\langle {}^2\Sigma_g | \mu_1 | {}^2\Pi_u \rangle$ transition, yield a sum which is almost equal to the result without spin–orbit coupling. However, the T_0 component, which is entirely due to spin–orbit effects, dominates the total calculated cross section. T_0 includes the $\langle {}^2\Sigma_g^+ | \mu_0 | {}^2\Sigma_u^+ \rangle$ and $\langle {}^2\Pi_g | \mu_0 | {}^2\Pi_u \rangle$ transition moments as shown in Eq. (IV.12a). Although these transition moments are multiplied by small coefficients, their magnitude causes them to be substantially more important than the $\langle {}^2\Sigma_g^+ | \mu_1 | {}^2\Pi_u \rangle$ moment which is multiplied by a factor near unity.

Even with spin–orbit effects included the total calculated cross section is seen to be in serious disagreement with experiment (about a factor of 3). There are several possible explanations for this disagreement. The calculated potential energy curves could contain errors that would cause the calculated absorption profile to shift to the red, thus bringing the left hand limb into better agreement with the experimental data. However, recent continuation of the experiments[15] has allowed estimates of the peak of the profile to be made. The experimental peak is at 716 nm, which is in near-perfect agreement with the calculated maximum. Hence, shifting of the potential energy curves to obtain agreement seems unlikely.

A second possible source of error is the assumption that the spin–orbit matrix element in Eq. (II.8) is independent of internuclear separation. There are two possible effects which could make this assumption invalid. First, the spin–orbit coupling constant α could change with R due to orbital distortion and two-center effects. However, since the principal part of α is an integral over r^{-3}, where r is the electronic coordinate, the integrand should be highly localized and should deviate significantly from the atomic value only at very small internuclear separations. Second, the expectation value of $\mathbf{l}_i \cdot \mathbf{s}_i$ for each electron can vary with R due to changes in the p character of the orbitals in the molecular overlap region. Our single configuration wavefunctions show only insignificant mixing of s and d components in the p orbitals. So, unless the molecular wavefunction is not adequately described by a single configuration at R_e, we do not expect significant variations in $\mathbf{l}_i \cdot \mathbf{s}_i$.

The third possible source of error is the calculated $^2\Sigma_u^+ - {}^2\Sigma_g^+$ and $^2\Pi_u - {}^2\Pi_g$ transition moments. As discussed in Sec. III these moments are approximately equal to $R/2$ even at internuclear separations near R_e. However, as pointed out in Sec. II the single configuration wavefunctions do not correctly account for the differences in the atomic orbitals between Ar and Ar^+. A more appropriate calculation would include either a large number of configurations or a nonorthogonal orbital formalism. Significant configuration interaction near R_e could alter substantially the computed transition moments. If all of the error in the computed cross sections were ascribed to the transition moments, then they could be in error by as much as $\sqrt{3}$. It is more likely, however, that a combination of errors in the transition moments and spin–orbit matrix elements is the source of the disagreement.

Figure 5 shows the effect of temperature on the computed cross section. Higher temperatures tend to broaden the profile and shift the maximum to the red as higher vibrational levels of the $^2\Sigma_u^+$ state are populated.

2. The $^2\Sigma_u^+ \rightarrow {}^2\Sigma_g^+$ transition

The effect of spin–orbit coupling on the $^2\Sigma_u^+ - {}^2\Sigma_g^+$ transition is negligible. Of all the terms contributing to the cross section in Eqs. (IV.7) and (IV.13) the $\langle {}^2\Sigma_u^+ | \mu_0 | {}^2\Sigma_g^+ \rangle$ term is totally dominant. Figure 6 shows our calculated absorption cross sections as a function of temperature. Also shown is the effect of the rotational quantum number J. Higher J values tend to broaden the red side of the profile slightly. The effect is small, however, and we are confident that the neglect of rotational effects as in Eq. (IV.15) is a good approximation.

Unfortunately, there are no published measurements of the uv absorption cross section in Ar_2^+ with which we can compare our data. Since the results for the visible band are in good agreement with experiment so far as wavelength is concerned, we feel that the position of the uv band is also reliable. Spin–orbit effects are insignif-

icant for this transition, so the approximations made in the spin–orbit analysis of Sec. II are of no consequence. This leaves only the question of the accuracy of the calculated transition dipole moments for the $^2\Sigma_u^+ \rightarrow {}^2\Sigma_g^+$ transition. As discussed in Sec. IV. B. 2 there are reasons to believe that the transition moments could change significantly for a more sophisticated calculation of the wavefunctions. If all of the error in the visible absorption band were ascribed to the transition moments, then we would have to conclude that the uv cross sections are too large by a factor of 3. More importantly, however, it is difficult to imagine any corrections which would cause the calculated cross sections to become larger.

The Ar_2^+ uv absorptions are very important in the modeling of rare-gas halide laser systems[16] where argon is used as the primary buffer gas. KrF, XeBr, XeCl, and XeF all lase at wavelengths which are encompassed by the Ar_2^+ uv absorption profile. Thus, their potential efficiencies and scalabilities are seriously affected by the results given here.

V. CONCLUDING REMARKS

It has been shown via direct *ab initio* calculations that there are no significant visible absorption cross sections involving the $^2\Sigma_u^+$ ground state of Ar_2^+. A maximum cross section of 2.6×10^{-19} cm^2 at 300 K for the $^2\Sigma_u^+ \rightarrow {}^2\Pi_g$ transition centered at 716 nm has been calculated, which is about a factor of 3 larger than the experimental measurements of Miller *et al.*[4] The $^2\Sigma_u^+ \rightarrow {}^2\Pi_g$ transition is dominated by spin–orbit effects, which were included in the calculations in an approximate way.

A very strong continuum absorption in the uv due to the $^2\Sigma_u^+ \rightarrow {}^2\Sigma_g^+$ dissociative transition has been theoretically characterized. A maximum cross section at 300 K of 0.5×10^{-16} cm^2 centered at 300 nm with a 75 nm FWHM has been calculated. Based on the comparison of the calculated visible absorption cross sections with experiment the predicted uv cross sections could be too large by as much as a factor of 3.

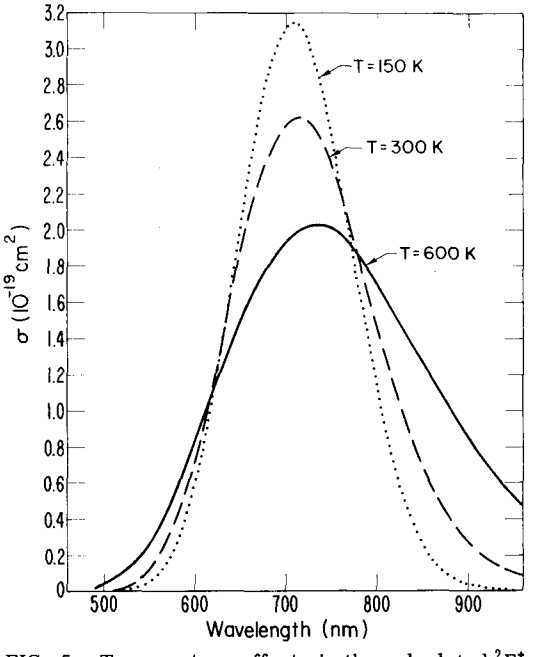

FIG. 5. Temperature effects in the calculated $^2\Sigma_u^+ \rightarrow {}^2\Pi_g$ absorption cross sections.

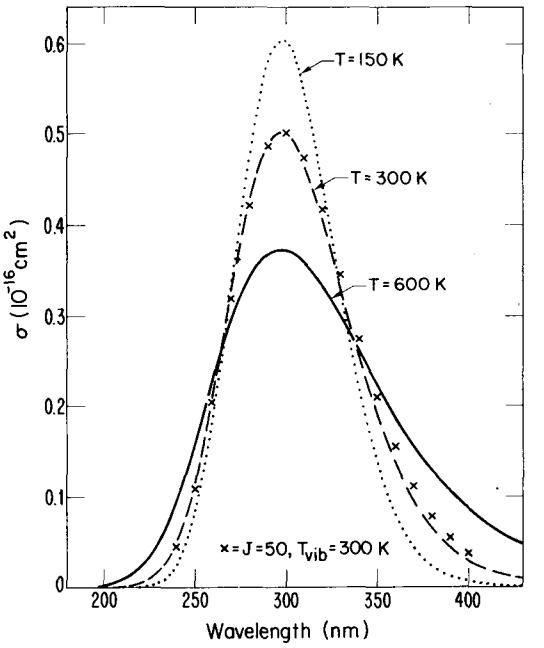

FIG. 6. Absorption cross sections for the $^2\Sigma_u^+ \rightarrow {}^2\Sigma_g^+$ transition in Ar_2^+. The X's represent the effect of rotational excitation ($J = 50$).

[1] C. K. Rhodes and A. Szöke, *Laser Handbook*, edited by F. T. Arecchi and E. O. Schuly-DuBois (North-Holland, Amsterdam, 1972).

[2] H. T. Powell, J. R. Murray, and C. K. Rhodes, Appl. Phys. Lett. **25**, 730 (1974).

[3] D. L. Huestis and E. Zamir, Quarterly Report No. 1, ERDA Contract No. E(04-3)-115, Stanford Research Institute, Menlo Park, CA 94025 (1976); Laser Fusion Division Final Report, Lawrence Livermore Laboratory, Livermore, CA 94550 (1975).

[4] T. M. Miller, J. H. Ling, R. P. Saxon, and J. T. Moseley, Phys. Rev. A **13**, 2171 (1976).

[5] T. L. Gilbert and A. C. Wahl, J. Chem. Phys. **47**, 3425 (1967).

[6] A. C. Wahl, J. Chem. Phys. **41**, 2600 (1964); G. Das and A. C. Wahl, Argonne National Laboratory Report No. ANL-7955 (1972).

[7] P. S. Bagus, T. L. Gilbert, and C. C. J. Roothaan, J. Chem. Phys. **56**, 5195 (1972).

[8] D. C. Lorents, R. E. Olson, and G. M. Conklin, Chem. Phys. Lett. **20**, 589 (1972).

[9] R. S. Mulliken, J. Chem. Phys. **52**, 5170 (1970).

[10] M. Krauss, Natl. Bur. Stand. Tech. Rep. **438** (1967).

[11] H.-U. Mittmann and H.-P. Weise, Z. Naturforsch. Teil A **29**, 400 (1974).

[12] I. V. Kosinskaya and L. P. Polozova, Opt. Spectrosc. **30**, 458 (1971).

[13] In their paper Miller *et al.* estimate $\mu^2 = 0.009$ a.u., but in a private communication we were informed that this value includes a degeneracy factor of 2 for the $^2\Pi_g$ state.

[14] R. G. Gordon, J. Chem. Phys. **51**, 14 (1969).

[15] T. Miller (private communication).

[16] For rare-gas/halide lasers see, for example, S. K. Searles and G. A. Hart, Appl. Phys. Lett. **27**, 243 (1975); J. J. Ewing and C. A. Brau, Appl. Phys. Lett. **27**, 351 (1975); E. R. Ault, R. S. Bradford, and M. L. Bhaumik, Appl. Phys. Lett. **27**, 413 (1975); C. A. Brau and J. J. Ewing, Appl. Phys. Lett. **27**, 435 (1975).